Normal band 3—cytoskeletal interactions are maintained on tanktreading erythrocytes

Frances E. Weaver,* Heike Polster,* Peter Febboriello,* Michael P. Sheetz,‡
Holger Schmid-Schonbein,§ and Dennis E. Koppel*

*Department of Biochemistry, University of Connecticut Health Center, Farmington, Connecticut 06032; ‡Department of Cell Biology and Physiology, Washington University Medical School, St. Louis, Missouri 63110 USA; and §Reineland-Westphalia Technical University, D5100 Aachen, Federal Republic of Germany

ABSTRACT Normal nonnucleated erythrocytes subjected to continuous hydrodynamic shear exhibit membrane deformation or "tanktreading," a process important for reduction of the bulk viscosity of circulating blood. To characterize the effect of this unique process on the erythrocyte membrane we have measured the lateral diffusion of band 3 during tanktreading. Band 3 is normally constrained through interactions with the spectrin-actin cytoskeleton, therefore, any significant disruption of these interactions would result in alterations in band 3 dynamics. Band 3 of human erythrocytes was labeled with dichlorotriazinyl amino fluorescein. After laser photobleaching of an equatorial stripe, fluorescence images were recorded from cells in the presence or absence of shear. The amplitude of induced nonuniformity in the surface distribution of fluorescence was calculated directly from images of unsheared cells. In shear the bleached line rotated with the tanktreading motion of the cells. The surface integral of fluorescence oscillated with this motion. For this case, the amplitude of photobleaching-induced nonuniformity was defined as the amplitude at the fundamental frequency of fast Fourier transforms in time of the oscillations. Shear stress–induced membrane flow did not interrupt the linkage of band 3 with the erythrocyte cytoskeleton. Diffusion coefficient and mobile fraction ($1.5 \pm 0.5 \times 10^{-10}$ cm^2/s and $54 \pm 11\%$, respectively) were unaffected by shear. The rate of fluorescence recovery of cells in shear was also similar at the centers and at the edges, where in-plane shear forces are maximal.

INTRODUCTION

Proteins in native membranes rarely diffuse at the rates predicted by fluid dynamic theories for free diffusion in a lipid bilayer (Saffman and Delbruck, 1975). Interactions with the cytoskeleton (Fowler and Bennett, 1978; Koppel et al., 1981; Sheetz et al., 1980; Golan and Veatch, 1980; Smith and Palek, 1982; Tank et al., 1982), the extracellular matrix (Weir and Edidin, 1986), and the glycocalyx (Weir and Edidin, 1988) have been implicated in restricting diffusion. The extremely limited diffusion of erythrocyte membrane glycoproteins in normal cells appears to be due to their association with the cytoskeleton. In particular the anion transporter, band 3, is tethered to or corralled within the cytoskeletal network. In spectrin-deficient mouse erythrocytes, however, band 3 exhibits near free diffusion, limited only by the viscosity of the lipid bilayer (Sheetz et al., 1980; Koppel et al., 1981). Treatments which partially dissociate spectrin from itself or from ankyrin (Schindler et al., 1980) or ankyrin from band 3 (Fowler and Bennet, 1978) result in increased mobility of band 3 in human erythrocytes, whereas cross-linking of spectrin with diamide reduces mobility (Smith and Palek, 1982). As reviewed by Sheetz (1983), these studies suggest that band 3 diffusion is restricted both by linkage of (immobile) band 3 to the cytoskeleton as well as by steric hindrance of the mobile population.

The erythrocyte cytoskeleton is also responsible for the maintenance of cell shape and viscoelastic properties. Certain diseases and pharmacological agents which perturb cytoskeletal linkages and alter the cell shape affect the ability of the cell to tolerate mechanical stress (reviewed by Bennett, 1985; Chasis and Mohandas, 1986). In shape altering diseases, this lack of deformability results in early destruction in the circulation. The deformability of the normal red cell is so high that in model systems (Schmid-Schonbein and Wells, 1969; Schmid-Schonbein et al., 1973; Fischer et al., 1978; Chasis and Mohandas, 1986) it can be shown to extend into a prolate ellipsoid with the length of the long axis up to three times that of the original diameter of the biconcave disk. Elongation occurs at forces and viscosities similar to those found in normal circulating plasma (Schmid-Schonbein, 1981). By visualization or cytoplasmic inclusions (Heinz bodies) and beads adhering to the membrane it has been demonstrated that, when elongated in continuous shear, the erythrocyte's membrane moves

Address correspondence to Dr. Weaver at Division of Cardiology, Brigham and Women's Hospital, 75 Francis St. Boston, MA 02115.
Dr. Polster's current address is Dept. of Pediatrics, George August University, Gottingen, FRG.

0006-3495/90/12/1427/10 $2.00

around its cytoplasm much as the tread of a tank rolls around the wheels (tanktreading, Fischer et al., 1978). This process dissipates energy into the cytoplasm forcing it to flow. Yet when released from shear the cells immediately return to their normal discoidal shape.

Elastic memory and the ability to deform appear to be functions of the intact erythrocyte cytoskeleton. Spectrin-deficient mouse cells fragment in shear (Schmid-Schonbein, 1983). Erythrocytes with cross-linked spectrin (Schmid-Schonbein, 1983, Chasis and Mohandas, 1986), or photodamaged cells (personal observations) buckle in shear and do not elongate. Vesicles fragmented by shear from normal cells have lipid and protein compositions identical to those of intact cells suggesting that tanktreading is not the result of wholesale blebbing of the membrane away from the cytoskeleton (Chasis and Mohandas, 1986). Yet lipid vesicles separated by shear from ATP-depleted cells do not contain spectrin (Lutz, 1978). Subtle alterations in the equilibrium of membrane-cytoskeletal associations in ATP-replete cells would not necessarily result in changes in composition.

Whereas the effects of shear on the normal erythrocyte cytoskeleton and its membrane linkages have remained unclear, several models can be proposed. The cytoskeleton may move in concert with the membrane over the cytosol, membrane-cytoskeletal interactions remaining intact. Membrane-skeleton linkages may be constantly breaking and reforming as the cell is sheared. A theoretical study of the behavior of membrane "elements" in shear has suggested a "periodic in-plane gliding" associated with marked bending and extension with high frequencies (Schmid-Schonbein, 1983) which might result from local unfolding of the protein network or temporary dissociation of protein–protein interactions. The membrane might be released completely from the cytoskeleton and move independently of it. In this case, membrane proteins would be free to intermix at rates influenced only by the viscosity of the bilayer. Finally, an active stirring or membrane components could occur, causing intermixing of protein and lipids at rates higher than expected for diffusion alone.

To take advantage of band 3's known interaction with cytoskeletal components in assessing the effect of shear on the status of the erythrocyte membrane, we have monitored the lateral diffusion of fluorescently tagged band 3 as a function of shear stress and as a function of position along the cell axis perpendicular to the direction of shear. The disruptive processes described above were expected to result in increases in the lateral diffusion rate of band 3 or in reductions in the numbers of immobilized proteins. Such effects should be proportional to the rate of shear, and, under the same shear rate, to the energy dissipation (Fischer, 1980) or membrane stress resultants (Tran-Son-Tay et al., 1987) which are maximal in the lateral margins of the cell.

SAMPLE PREPARATION

Materials

Dextran 70,000 was obtained from Sigma Chemical Co. (St. Louis, MO). Dichlorotriazinyl amino fluorescein (DTAF) was obtained from Molecular Probes Inc. (Eugene, OR), *N*-4-nitrobenzo-2-oxa-1,3, diazole phosphatidylethanolamine (NBD-PE) was from Avanti Polar Lipids Inc. (Birmingham, AL). All other chemicals were from Sigma Chemical Co.

Methods

Preparation of erythrocytes. Venous blood was collected from healthy human donors into sodium citrate anticoagulant, centrifuged at 1,200 *g* for 10 min, and the serum and buffy coat were aspirated. A small volume of the remaining erythrocytes was washed once at 1:100 dilution in phosphate-buffered saline (PBS, 10 mM sodium phosphate, 135 mM NaCl, pH 7.4), by spinning 10 s in a Fisher Scientific Co. (Pittsburgh, PA) microcentrifuge, model 235A.

Labeling of band 3. Prewashed cells at 20% hematocrit were incubated with an equal volume of 1 mg/ml DTAF in 0.2 M sodium borate, pH 9.7 for 20 min on ice. Labeled cells were washed three times with PBS containing 1 mg/ml bovine serum albumin (BSA), and resuspended to 30% hematocrit in PBS, 1 mg/ml BSA, 10 mM glucose, pH 7.4. Labeling of band 3 was confirmed by gel electrophoresis (data not shown). As has been previously noted (Sheetz et al., 1980), this procedure resulted in 80% of the DTAF label attached to band 3 with the remainder largely on the glycophorins.

Labeling with lipid analogue. To assess the ability of the video image analysis system to measure the surface distribution of species with diffusion coefficients in excess of 10^{-10} cm^2/s, separate aliquots of cells were labeled with the rapidly diffusing lipid analogue NBD-PE. 2 μl of NBD-PE at 1 mg/ml in absolute ethanol were incubated with 1 ml of prewashed cells at 1% hematocrit in PBS, 10 mM glucose for 30 min at 37°. To ensure adequate removal of free probe, cells were washed a total of 12 times in PBS, 10 mM glucose, 1 mg/ml BSA, pelleting for 10 s in the microcentrifuge each time. Between each of the second through the fifth washes cells were resuspended and held on ice for 5 min before pelleting. Finally labeled cells were resuspended to 30% hematocrit in PBS, 10 mM glucose, 1 mg/ml BSA.

Preparation of high-viscosity dextran. Dextran 70,000 was dissolved in deionized water at 20–50% (wt/vol) and dialyzed against deionized water for 3 d. The viscosity of this solution was measured by capillary viscometry, and it was mixed 15:1 with concentrated potassium phosphate saline (13.2 mM Na_2HPO_4, 1.7 mM NaH_2PO_4, 90.5 mM KCl, 44.6 mM NaCl). The pH was adjusted to 7.4, the osmolality was measured by freezing point osmometry and adjusted to 295, and the final viscosity determined. A single preparation of 57 cpoise dextran was used throughout these experiments.

Conditions of fluorescence redistribution after photobleaching (FRAP) experiments. Immediately before FRAP experiments, labeled cells were added to buffered dextran to a final hematocrit of 5%. 2-Mercaptoethylamine (cysteamine) was added to a final concentration of 15–30 mM to minimize photodamage, and the sample was made 16–32 mM in sodium salicylate to counteract stomatocytogenic effects of cysteamine. 5 μl of the cell suspension were then added to the rheoscope chamber. Measurements were made at 22°C.

FLUORESCENCE REDISTRIBUTION AFTER PHOTOBLEACING

Optical instrument

The shear-induced behavior of a suspension of red cells in the rheoscope has been described previously (Schmid-Schonbein, 1973; Fischer, 1978). The rheoscopic chamber, consisting of a transparent plastic cone which counter-rotates with a glass plate, is mounted on a inverted microscope (Diavert, Leitz, FRG). Cells suspended midway between cone and plate remain stationary relative to the observer during short periods of shear. The objective mount was replaced with the illuminator head of a Leitz Ortholux fluorescence microscope. As shown in Fig. 1, the 4880 A line of a 4W Lexel argon laser (Cooper Lasersonics, Inc., Palo Alto, CA) was directed via mirrors M1 and M2 to the first plate of a beamsplitter/shutter device (described in Koppel, 1979, 1986) and used for both bleaching and monitoring. A cylindrical lens (L1) focused the unattenuated beam in one dimension to a line for localized bleaching. The total power of the attenuated beam, which illuminated a circular area several cell diameters across for video monitoring, was increased ~100-fold (over the usual 10,000-fold attenuation used when the two beams have the same profiles) by coupling two mirrors (M3 and M4) to the surfaces of the beamsplitter plates with immersion oil. Both beams were focused at the back of the illuminator via a 40 mm focal length lens (L2). A 63×, 0.85 NA objective focused the beams onto the cells, collected and imaged the resulting fluorescence. Electronic shutters controlled the periods of bleaching and monitoring illumination, and protected the camera from illumination during the bleaching pulse.

For video microscopy a 5× photo ocular was inserted into the photoport of the rheoscope as a relay lens to an image intensifier coupled to a silicon intensified target (SIT) camera (Dage-MTI Inc., Wabash, MI). The video signal was fed through a time-date generator equipped with a stop watch function to uniquely identify every frame. All video data were recorded on a AG6300 VHS recorder (Panasonic Co., Secaucus, NJ) for subsequent playback and analysis.

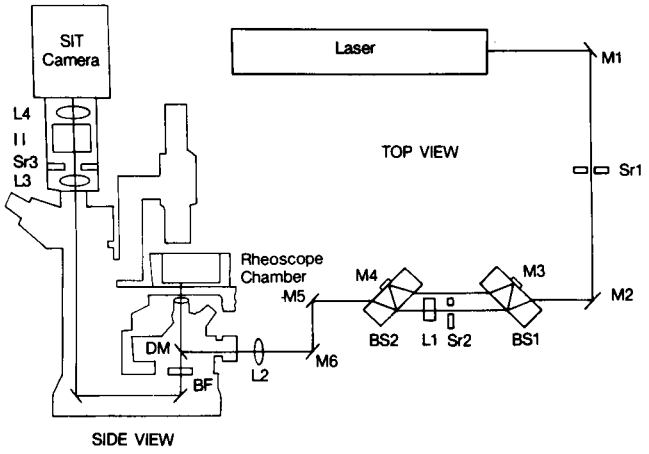

FIGURE 1 Modification of the optical bench for video FRAP experiments using the rheoscope as described in Methods, optical instrument.

General strategies

Bleaching a stripe across the full width of the cell at its center (along axis *b* in Fig. 2), perpendicular to the direction of shear, offered several advantages. With the bleaching beam several cell diameters across in one dimension, proper sample alignment required fine positioning in only one dimension, and allowed us to determine localized diffusion rates, comparing areas exposed to varying degrees of shear (i.e., the lateral margins versus the center).

Low-light-level video was used for data recording to permit the analysis of fluorescence redistribution after photobleaching on individual continuously tanktreading cells. Series of fluorescence images encompassing several tanktreading cycles were recorded. Subsequently, the continuing extent of photobleaching-induced nonuniformity was determined for each series of images.

For data analysis, this method is capable of efficiently handling the enormous volume of data generated with a minimum of operator intervention. Each video tape seg-

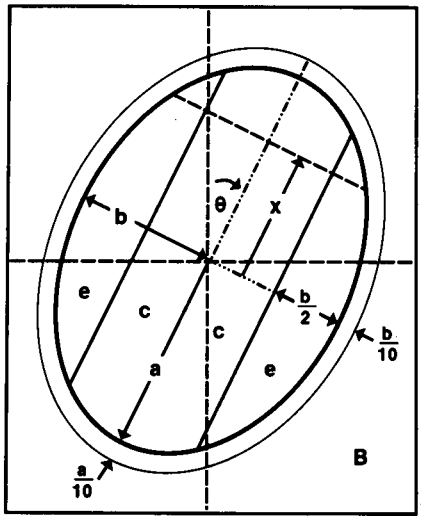

FIGURE 2 Geometry of a tanktreading cell. *a* and *b* are the semimajor and semiminor axes of the elliptical projection, *e* and *c* mark the areas of edge and central surface integration. Theta is the angle of rotation relative to the screen axis. *B* = area of integration for background fluorescence.

ment of 5 s of illumination in a single tanktreading sequence consists of 150 frames; equaling 36.9 Mbytes of information per single time point once digitized. The analysis ultimately reduces this to three floating-point numbers. Data from tanktreading and stationary cells were treated in comparable fashions, and we were able to make localized measurements in the cell center and lateral edges. Finally, the analysis also compensated for the effects of photobleaching during monitoring. With the probes and detectors used, a certain amount of photobleaching during monitoring was unavoidable. For these purposes, we adopted an approximate form of the normal-mode analysis of lateral diffusion on a bounded membrane surface (Koppel, 1985), as described below.

Experimental protocols

Under incandescent light, a cell was positioned so that its center corresponded with the position of the center of the bleaching line. At this point, the VCR was started to record continuously throughout the experiment. A prebleach fluorescence image was taken with 2 s of monitoring laser illumination at manual gain of the SIT camera. We had previously determined that the camera response was linear at the range of gain settings used. The same manual gain settings were maintained throughout a single day's experiments. The camera was shuttered off and a 10-ms bleaching laser pulse was applied. Although a number of cells in the field were bleached, only the single cell centered on the bleaching beam was followed and analyzed.

After bleaching, DTAF labeled cells (tanktreading and stationary) were illuminated with the expanded monitoring laser beam for 5 s every 30 s. The cells were followed in brightfield illumination (with the camera switched to automatic gain) during the intervening periods. Only those cells that showed no evidence of photodamage, as detected by the absence of buckling during periods of shear, were analyzed.

In studies of tanktreading cells, a 2-s postbleach fluorescence image of the cell was recorded before tanktreading was initiated. Subsequently, cells were continuously exposed to shear. One group of cells was exposed to low shear (shear stress, ~8 dyn/cm^2; shear rate, ~4/s; elongation, 20–50% of maximal) throughout the experiment. Others were exposed to high shear (shear stress, ~40 dyn/cm^2; shear rate, ~70/s; elongation, 60–80% of maximal, greater than 2:1 elongation) during the intervening periods, but low shear during fluorescence imaging.

Similar bleaching conditions were employed for cells labeled with the lipid analogue NBD-PE. Fluorescence redistribution was so rapid that only stationary cells could be studied. Beginning immediately after bleaching, NBD-PE labeled cells were continuously illuminated with the expanded monitoring laser beam for 20 s. Some of these cells became stomatocytes after bleaching; only those that did not change shape were analyzed.

For data playback, digitization, and analysis, the VHS recorder was coupled to a digital image processor (Recognition Technology Inc., Holliston, MA), with an IBM-PC/AT serving at host computer (IBM Instruments Inc., IBM Corp., Danburg CT). A computer control board was constructed that mimicked the operation of the wired VCR remote controller.

For the analysis of a tanktreading sequence, the computer advanced the VHS recorder frame by frame, and directed the image processor to digitize each frame and compute a series of four-frame averages. As the average period of the tanktreading cycle was 1.74 s (52.2 frames) this represented an average over 0.08 periods, giving a fourfold decrease in the volume of data and a twofold increase in signal-to-noise without significant loss of time resolution. The area of a single cell represented <5% of the full frame, therefore, we further reduced the volume of data, and eliminated much of the stray light from other cells in the field, by storing only a small, rectangular "area-of-interest" centered around each cell. The remainder of stray illumination was corrected for during background subtraction. Images which were blurred due to stage movement or loss of focus were rejected at this point.

Images taken of stationary, unsheared cells were processed and stored in a similar fashion. Data for NBD-PE-labeled cells were stored as a series of contiguous 16-frame averages. At each time point, single images of stationary DTAF-labeled cells were computed as averages of 64 or 128 consecutive frames.

Data analysis theory

We characterize $c(\sigma, t)$, the distribution of fluorescent molecules on the cell surface at time t, through calculations of the normalized second moment, which we define as:

$$M_2^{(s)}(t) = \langle x^2 \rangle_s = \int_s x^2\, c(\sigma, t)\, d^2\sigma \Big/ \int_s c(\sigma, t)\, d^2\sigma, \quad (1)$$

where x ($-1 \le x \le 1$) is the distance from the cell center perpendicular to the bleached line (in the direction of tanktreading) normalized by the radius of the cell along this axis, and s specifies the area covered by the integral over the surface of the cell. As indicated in Fig. 2, we designate integrals over the whole surface (within the bold oval of Fig. 2), the central 50% of the cell width (areas c) and the outermost 50% of the cell width (25% on each edge, areas e in Fig. 2) as $s = w, c$, and e (for whole,

center, and edge), respectively. The normalization integral in the denominator of Eq. 1 corrects for the effects of bleaching by the monitoring beam.

Bleaching a line across the center of the cell (where by definition x is near zero) will increase the value of the second moment over its initial prebleach value on uniform cells. For stationary cells, then, we can define a function $A_2(t)$ as a measure of the photobleaching-induced nonuniformity:

$$A_2^{(s)}(t) = M_2^{(s)}(t) - M_2^{(s)}(-), \quad (2)$$

where $(-)$ specifies the prebleach value.

For the surface of a sphere, $A_2^{(w)}(t)$ has a known analytical form. In this case, $M_2^{(w)}(-)$ has the solution $1/3$ for a sphere of uniform intensity, (or a uniformly labeled spherocytic erythrocyte, Koppel, 1980) so that

$$A_2^{(w)}(t) = (2/3)\langle P_2(x)\rangle_w, \quad (3)$$

where $P_2(x) = 1/2\ (3x^2 - 1)$ is the 2nd-order Legendre polynomial. By normal-mode analysis (Koppel, 1985), we then know that $A_2^{(w)}(t)$ decays exponentially due to the diffusion with a decay rate proportional to diffusion coefficient D, and inversely proportional to the square of the effective radius a:

$$A_2^{(w)}(t) = A_2^{(w)}(0) \exp(-6Dt/a^2). \quad (4)$$

Although we do not have an analytical form of $A_2^{(s)}(t)$ for the complex geometry of the erythrocyte membrane, it has already been shown that the decay rate of $A_2^{(s)}(t)$ can be used as an empirical measure of the rate of the diffusion-mediated redistribution back to uniformity (Koppel, 1985).

It was not possible to stop tanktreading cells so that the bleached line was exactly in its original position and record single images. Any rotation or misalignment of the bleached areas on the upper and lower surfaces of the cell would be difficult to distinguish from diffusional broadening. For tanktreading cells, therefore, we are better served by a different definition of $A_2^{(s)}(t)$. $M_2^{(s)}(t)$, calculated from each stored image in a tanktreading sequence, oscillates periodically for bleached, tanktreading cells, but not for uniformly labeled cells (see Results). $M_2^{(s)}t$ reaches a maximum when calculated from those images in which the bleached line is along axis b in Fig. 2, and a minimum when it is at the periphery. As our measure of photobleaching-induced nonuniformity, in this case, the oscillations in $M_2^{(s)}(t)$ were fit to sums of sine waves using fast Fourier transforms in time. $A_2^{(s)}(t)$ was defined as the amplitude of the periodic modulation calculated at the fundamental frequency of the transforms.

Data analysis methods

We make the assumption that the membrane fluorescence recorded within a given pixel in the two-dimensional image array is simply proportional to the product of the illuminating intensity, the surface concentration of unbleached fluorophore, and the surface area of membrane within the pixel. In this case, experimental estimates of the surface integrals specified in Eq. 1 can be computed as simple sums of the form: $\Sigma\Sigma m_{ij}^{(s)}\ (x_{ij})^k\ (F_{ij} - B)/I_{ij}$, with $k = 0$ or 2. Here x_{ij} and F_{ij} are the values of x (see Eq. 1), and the fluorescence intensities, respectively, at the ith, jth pixel position, B is the average background intensity level, and m_{ij} is an array of 1's and 0's which masks the desired area of the cell. The values of I_{ij} are taken from an image of a thin, uniform layer of dye solution. B is calculated for each image as the average intensity in the area surrounding the cell. To normalize for bleaching during monitoring, the result when $k = 2$ is then divided by the result when $k = 0$. Calculations of $m_{ij}^{(s)}$ and x_{ij} take into account the lengths of the semimajor and semiminor axes of the projected cell image (modeled as an ellipse), the angle between the major axis and the image vertical, and the aspect ratio of the digitized video frame. To minimize computation time, the arrays of the products $m_{ij}^{(s)}\ (x_{ij})^k$, the masks for each individual cell, are generated only once for each tanktreading series and stored as images in the digital framestore.

For each tanktreading sequence, $A_2^{(s)}(t)$, the measure of bleaching-induced nonuniformity, is taken as the amplitude of the periodic modulation of $M_2^{(s)}(t)$, calculated at the fundamental frequency of the fast Fourier transform of the oscillation. The data are interpolated with cubic splines to cover an integral number of periods with 32 points, and fast fourier transformed in time using the MathCAD software package (Mathsoft, Cambridge, MA). The fundamental period of oscillation is found by systematically varying the total time range of the interpolated data for whole-cell integrations ($s = w$) so as to maximize the modulation amplitude. For tanktreading and stationary cells, approximate values of D and percent recovery are calculated from nonlinear least squares best fits of $A_2^{(s)}(t)$ to exponential decays to baselines.

RESULTS

To demonstrate the decay in fluorescence depletion observed during the course of a FRAP experiment, images collected from an NBD-PE-labeled erythrocyte are shown in Fig. 3. Redistribution of fluorescence is rapid such that the edges of the bleached region become blurred to the eye within a few seconds ($B2$–$B4$). A substantial amount of bleaching of the entire cell also occurred during the

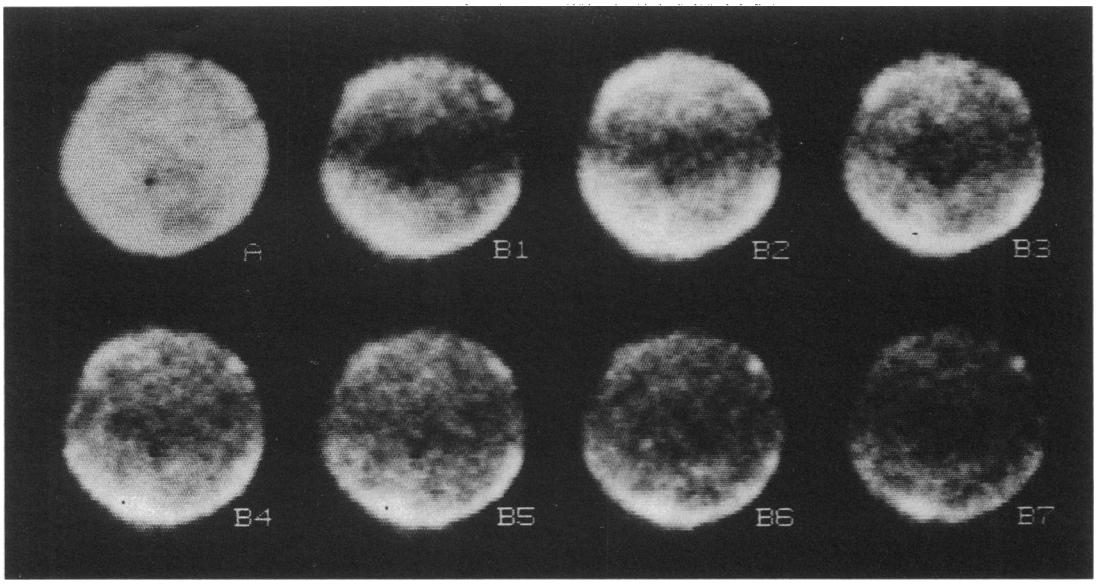

FIGURE 3 Images taken from the video screen of the course of a FRAP experiment on a NBD-PE labeled cell. Each image represents a four frame sum of the incoming video signal. (*A*) Prebleach image. (*B*1–*B*7) Images taken over the course of continuous illumination. Image *B*1 is 2 s postbleach, time between each of the images *B*1 through *B*7 is $4/30$ s.

monitoring period resulting in dimming of the entire cell (*B*4–*B*7). Each image corresponds to a single time point on the decay curve shown in Fig. 4. Similar images were collected from DTAF labeled stationary cells. Our analytical methodology compensated for any effects that uniform bleaching, as seen in Fig. 3, would have had on the calculation of $A_2^{(w)}(t)$.

The average decays in $A_2^{(w)}(t)$ of unsheared, DTAF-labeled cells and a representative unsheared, NBD-PE-labeled cell analyzed identically are shown in Fig. 4. The solid lines in Fig. 4 represent a nonlinear least squares best fit of $A_2^{(w)}(t)$ to an exponential decay plus a constant. Diffusion coefficients differed by two orders of magnitude as has been seen for the diffusion of band 3 and lipid probes using fluorescence redistribution after photobleaching (Koppel et al., 1981). Thus, we are confident that digitization of fluorescent images permits detection of differences in lateral diffusion rates.

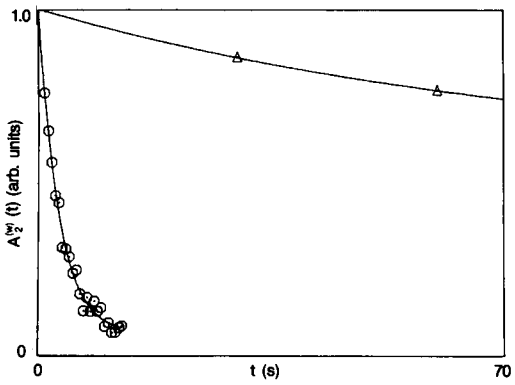

FIGURE 4 Plot of the decay of fluorescence depletion for lipid and protein labeled stationary cells. (*Triangles*) First two points of average protein decay, $N = 8$. Error bars have been eliminated for simplicity. (*Circles*) A single representative lipid labeled cell. Solid lines are the theoretical curves from nonlinear least squares fits of $A_2^{(s)}(t)$ to an exponential decay plus a constant.

The lag time between bleaching and initiation of tanktreading was much longer than the half time for lipid diffusion. Therefore, it was not possible to follow NBD-PE-labeled cells in the presence of shear. Fig. 5 demonstrates the course of a FRAP experiment on a DTAF-labeled tanktreading cell. Fig. 5 *A* is the prebleach image, 5 *B* = 2 s postbleach, and *C*1 is taken after the initiation of tanktreading. Note the elongation of the tanktreading cell relative to its resting diameter. Due to the wide depth of field of the objective relative to the cell thickness, the bleaching pulse destroyed the fluorophore on both sides of the cell. Tanktreading displays the complete surface distribution of fluorescence; a form of the bleached line appears at $x = 0$ (in the center of the cell) twice per cycle (Fig. 5, *C*1 and *C*9), and when the two sides of the bleached region reached $x = -1$ and $x = 1$ (Fig. 5, *C*4 and *C*5) the fluorescent image of the cell appears uniform and slightly smaller. This is due to the lack of signal from the perimeter (note the absence of the bleached region

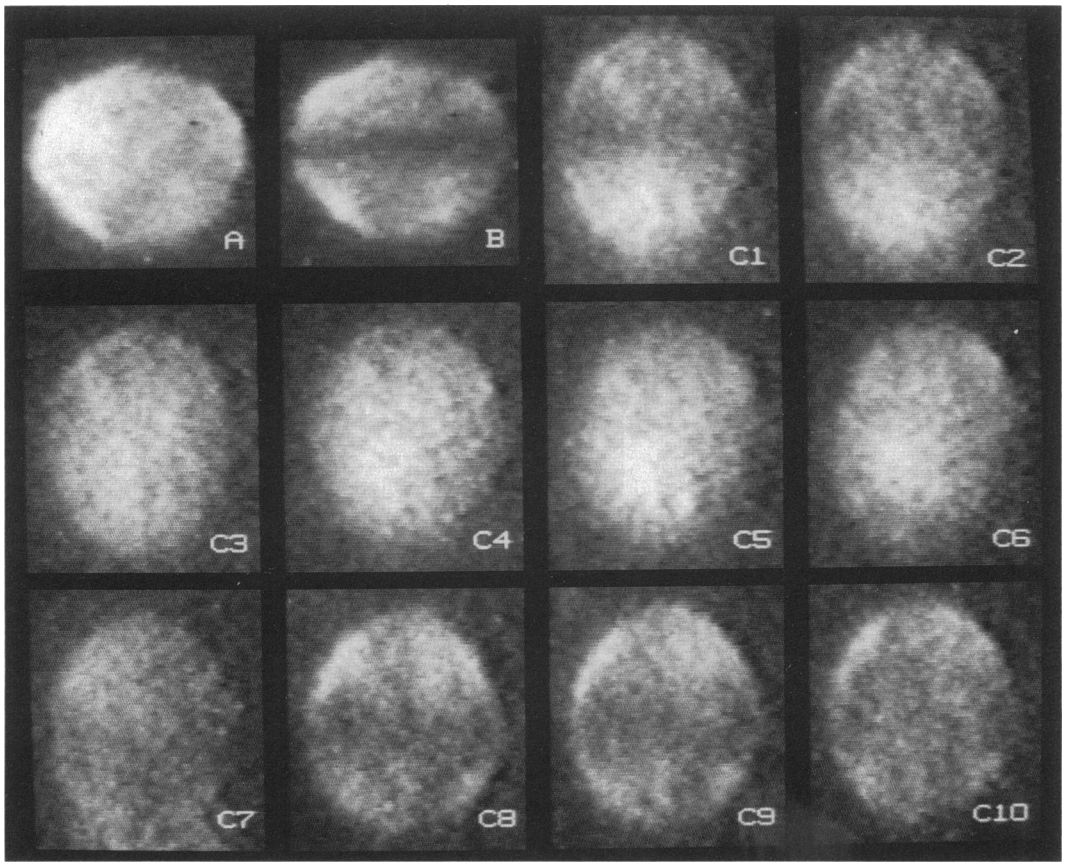

FIGURE 5 Images taken from video screen of the course of a FRAP experiment on a tanktreading erythrocyte. Each image represents a four frame sum of the incoming video signal. (*A*) prebleach image. (*B*) 2 s postbleach. *C*1 and *C*10 are a series of images taken after initiation of tanktreading in low shear. *C*1 is 22 s postbleach, time between images *C*3 and *C*4, and *C*7 to *C*8 is $^{8}/_{30}$ s; time between all other images *C* is $^{4}/_{30}$ s.

from the center of the cell). These images clearly show that the membrane does in fact move like a tank's tread, substantiating the interpretation of the latex bead–Heinz body experiments (see Introduction).

During tanktreading, bleached cells exhibited a maximum value of $M_2^{(s)}(t)$ when the bleached region was in the center of the cell (Fig. 5, *C*1) and a minimum when it was at the edge (Fig. 5, *C*4), the value of $M_2^{(s)}(t)$ oscillating over the period of tanktreading. A representative oscillation in $M_2^{(s)}(t)$ for the entire surface of a cell in low shear ($s = w$) is shown in Fig. 6. Each data point represents a single digitized image of the sort shown in Fig. 5. The average period of tanktreading in low shear was 1.74 s. This is at the low end of reported values for tanktreading frequency in dextran solutions (Fischer, 1980). Such a low frequency was required to achieve sufficient stability for extended periods of data collection. The solid line in Fig. 6 *A* is the cubic spline interpolation of the oscillation. The fast Fourier transform of the fundamental period of the oscillation to give the fundamental frequency is shown in Fig. 6 *B*. We refer to the height of the peak of the fundamental frequency as the modulation amplitude. Oscillations in $M_2^{(s)}(t)$, for s = whole surfaces (w), centers (c), and edges (e, see Fig. 2 and Methods) for cells in high shear and low shear were analyzed in a similar fashion.

The effect of shear on the average decay in modulation amplitude, $A_2^{(w)}$, of DTAF labeled cells is shown in Fig. 7. The solid lines represent the theoretical fit. The rate of decay of the modulation amplitude did not change significantly as a function of shear stress. Decay rates and mobile fractions were obtained from nonlinear least squares best fits of the average decay curves shown in Fig. 7. Based on the normal mode analysis theory developed by Koppel (1985), an effective radius (a) of 3.0 μm was estimated. The rate of decay of $A_2^{(s)}(t)$ was then converted to diffusion coefficients using Eq. 4. Mobile fractions were calculated by the method of Axelrod et al. (1976). As there were no significant differences in decay rates as a function of shear, an average decay curve was con-

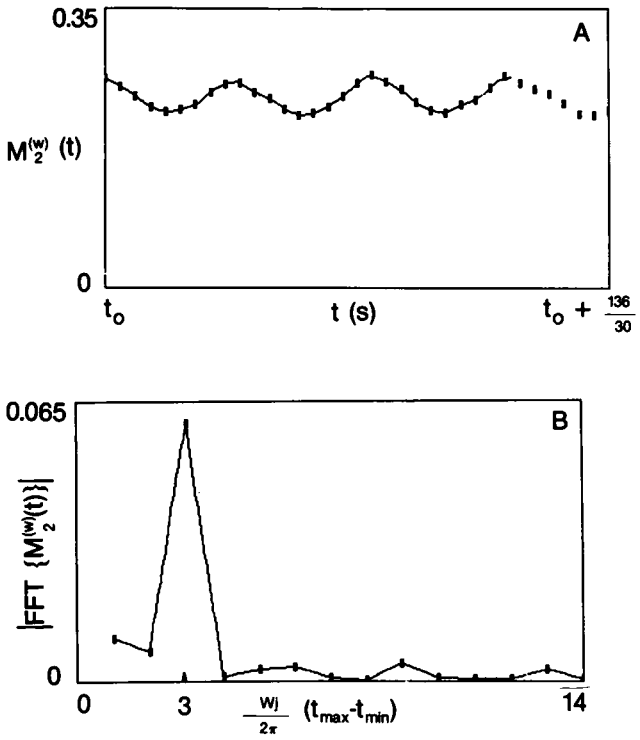

FIGURE 6 (*A*) Representative oscillation in $M_2^{(s)}(t)$ during tanktreading of a DTAF labeled cell in low shear. Squares are values of $M_2^{(s)}(t)$ for images taken at $\frac{1}{30}$ s intervals. Solid line is the cubic spline interpolation used for the Fourier transform. t_0 = initial frame of the sequence. 130/30, the total number of frames/30 frames s^{-1} = 4.33 s. (*B*) Peak of the transform, points connected for clarity. ($w_j/2\Pi$) ($t_{max} - t_{min}$) defines the frequencies of the transform, where t_{max} and t_{min} = the ending and starting points, respectively, of the tanktreading sequence shown in *A*. The fundamental frequency of the transforms equalled the period of tanktreading.

structed. The average diffusion coefficient and mobile fraction were 1.5 ± 0.5 × 10^{-10} cm^2/s and 55 ± 11% (n = 8 stationary, 10 low, and 5 high shear, from a total of 6 experiments using 6 different donors), respectively.

In-plane shear forces are maximal at the lateral edges of the cell perpendicular to the direction of shear (Fischer, 1980; Tran-Son-Tay, 1987). Therefore, the spectrin-actin network may have been locally rather than totally disrupted. To determine positional effects of shear on band 3 lateral diffusion, we calculated the average decay in modulation amplitude $A_2^{(s)}(t)$ as a function of distance along the minor axis, for high shear, the most stressed case. The areas of the appropriate surface integrals are *c* (center) and *e* (edge) in Fig. 2. As shown in Fig. 8, no significant differences in band 3 diffusion were detected between the outermost 50% of the cell width perpendicular to the tanktreading axis and the center. Identical results were obtained for stationary cells and those in low

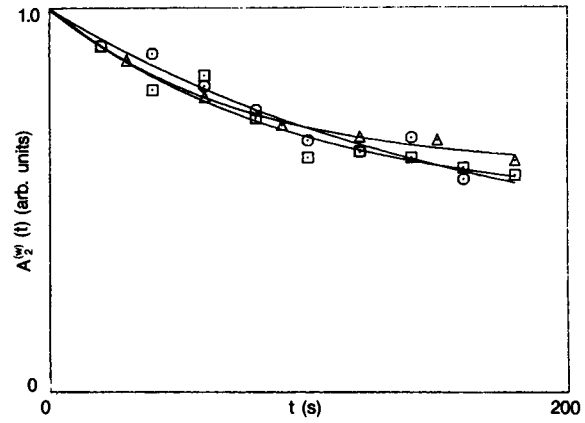

FIGURE 7 Effect of shear stress on the decay in modulation amplitude for DTAF-labled cells. (*Triangles*) Average of eight stationary cells; (*squares*) low shear, 8 dyn/cm, average of 10 cells; (*circles*) high shear, 40 dyn/cm, average of five cells. Error bars have been omitted for clarity. Solid line is the theoretical curve of the nonlinear least squares best fit of $A_2^{(s)}(t)$ to an exponential decay plus a constant.

shear (data not shown). The normal mode analysis used for the calculation of diffusion coefficients above is not applicable to geometry of the center and edge integrations, therefore, we did not attempt to estimate the diffusion coefficient or mobile fractions for these cases.

DISCUSSION

Using fluorescence redistribution after photobleaching combined with image processing we have measured the

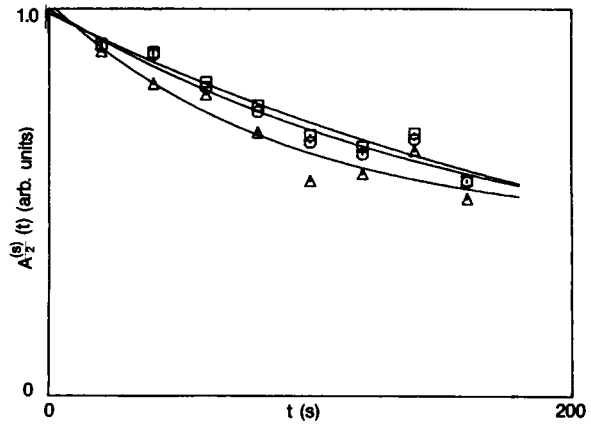

FIGURE 8 Decay in modulation amplitude of the centers and lateral margins of cells in high shear, error bars omitted for clarity. Solid line is the theoretical curve of the nonlinear least squares best fit of $A_2^{(s)}(t)$ to an exponential decay plus a constant. (*Circles*) Entire cell, (*squares*) centers, (*triangles*) edges.

lateral diffusion of band 3 in human erythrocytes subjected to continuous shear. We obtained similar estimates of diffusion coefficients for band 3 in the absence of shear as have been obtained by other photobleaching methods. However, our estimates are higher, by approximately a factor of four. This is most likely due to a discrepancy between our estimate of the effective radius for diffusion and the actual value if measured directly, and to approximations resulting from digitization. We show here that the shear stresses imposed on the human erythrocytes in the counter-rotating chamber of the rheoscope do not result in an appreciable release of restrictions to band 3 diffusion. These shear forces were in the lower range of tolerated and naturally occurring values (which can reach shear rates of 700/s in plasma; Fischer, 1980), suggesting that normal band 3–cytoskeletal interactions can persist when the erythrocyte experiences this type of stress in the circulation. As disruption of band 3–cytoskeletal interactions, or the spectrin network, by certain agents and in certain diseases results in release of restrictions to band 3 diffusion and alterations in the rheology and stability of the cells, our results offer further evidence that stable erythrocyte membrane–cytoskeletal associations are essential for survival in the circulation.

Because of the motion of the cells within the chamber, we were unable to extend our study to the upper limits of tolerated shear. Additionally, because of bleaching during recording, we were unable to measure lateral diffusion over very long times. Sheetz et al. (1980) have shown that the so-called immobile fraction of band 3 does diffuse if measurements are made at sufficiently long times after bleaching. A small decrease in immobile protein occurring with long term shear might have escaped detection in the present study. Sheetz (1983) has calculated that for a >10% dissociation of spectrin from actin the association constant must be decreased ~100-fold, with other cytoskeletal components also having extremely high association constants. Even at shear forces sufficient to fragment normal cells the proportions of membrane and cytoskeletal components in membrane fragments do not differ significantly from intact cells (Chasis and Mohandas, 1986). Therefore, it appears unlikely that the equilibria of cytoskeletal associations are significantly affected by shear.

Photobleaching in the absence of cysteamine under the conditions used here frequently resulted in cells which buckled in shear, reminiscent of the behavior of cells with spectrin cross-linked by diamide (Fischer et al., 1981). The necessity of including both cysteamine and sodium salicylate with the cells to prevent this photodamage may have introduced changes in the properties of the erythrocyte membrane. Stomatocytogenic agents, of which cysteamine is one, are believed to act by intercalating into the inner leaflet of the bilayer, thereby changing its curvature (Sheetz and Singer, 1974), with echinocytogenic agents acting on the outer leaflet. The influence of amphipath-induced shape changes on mechanical behavior is controversial, opposite effects on deformability having been obtained in media of different viscosities, and in different experimental systems (Mohandas and Shohet, 1978; Pfafferott et al., 1982; Reinhart and Chien, 1986). The consensus seems to be that under conditions of reversible shape change when no membrane area is lost, cellular deformability is identical to that of the biconcave disk, except at shear stresses <10 dyn/cm. In the present experiments, cells retained the biconcave disk shape, and no difference in the behavior of band 3 was detected between 8 and 40 dyn/cm. The effects echino- or stomatocytogenic agents which act at the lipid bilayer have on the lateral diffusion of membrane proteins have yet to be determined, although recent data suggest that the *distributions* of glycophorin and spectrin do change with amphipath-induced shape changes (Polster, unpublished results).

The largest amount of energy dissipated in shear is in the extreme lateral margins (10%) of the tanktreading cell (Fischer, 1980). Due to errors in focusing and in background subtraction due to cell associated fluorescence, we are able to analyze only the lateral 25%. Within this limitation, there appears to be no difference in band 3–cytoskeletal interactions at the lateral margins of cells in shear than in the central portion.

Our results are inconsistent with pulling of the entire membrane away from the cytoskeleton or with shear-induced mixing of membrane components. We suggest that the spectrin-actin network and the membrane undergo reversible extensions and compressions in tandem. Dissociations of the spectrin-actin network, if occurring, must result in transient openings in the network which are of shorter duration than is necessary to allow passage of slowly diffusing band 3. Thus, it appears from the present data that, as suggested by Elgsaeter et al. (1986), the erythrocyte membrane and cytoskeleton move as a unit when the cell is deformed in the normal circulation. The effect of shear on the dynamics of other membrane proteins and on the lipid bilayer remains a question for future study.

We thank Grant Fairbanks, David Chester, and David Wolf for critically reading the manuscript.

This investigation was supported by United States Public Health Services research grant GM23585 (DEK).

Received for publication 24 August 1989 and in final form 18 July 1990.

REFERENCES

Axelrod, D., D. E. Koppel, J. Schlessinger, E. Elson, and W. Webb. 1976. Mobility measurement by analysis of fluorescence photobleaching recovery kinetics. *Biophys. J.* 16:1055–1069.

Bennet, V. 1985. The membrane skeleton of human erythrocytes and its implications for more complex cells. *Annu. Rev. Biochem.* 54:273–304.

Chasis, J. A., and N. Mohandas. 1986. Erythrocyte membrane deformability and stability: two distinct membrane properties that are independently regulated by skeletal protein associations. *J. Cell Biol.* 103:343–350.

Elgsaeter, A., B. T. Stokke, A. Mikkelsen, and D. Branton. 1986. The molecular basis of erythrocyte shape. *Science (Wash. DC).* 234:1217–1223.

Fischer, T. M. 1980. On the energy dissipation in a tank-treading human red blood cell. *Biophys. J.* 32:863–868.

Fischer, T. M., M. Stohr-Leisen, and H. Schmid-Schonbein. 1978. The red cell as a fluid droplet: tank tread-like motion of the human erythrocyte membrane in shear flow. *Science (Wash. DC).* 202:894–896.

Fischer, T. M., C. W. M. Haest, M. Stohr-Leisen, and H. Schmid-Schonbein. 1981. The stress free shape of the red blood cell membrane. *Biophys. J.* 34:409–422.

Fowler, V., and V. Bennett. 1978. Association of spectrin with its membrane attachment site restricts lateral mobility of human erythrocyte integral membrane proteins. *J. Supramol. Struct.* 8:215–221.

Golan, D. E., and W. Vaetch. 1980. Lateral mobility of band 3 in the human erythrocyte membrane studies by fluorescence photobleaching recovery: evidence for control by cytoskeletal interactions. *Proc. Natl. Acad. Sci. USA.* 77:2537–2541.

Koppel, D. E. 1979. Fluorescence redistribution after photobleaching. A new multipoint analysis of membrane translational dynamics. *Biophys. J.* 28:281–292.

Koppel, D. E. 1980. Lateral diffusion in biological membranes. A normal mode analysis of diffusion on a spherical surface. *Biophys. J.* 30:187–192.

Koppel, D. E. 1981. Association dynamics and lateral transport in biological membranes. *J. Supramol. Struct.* 17:61–67.

Koppel, D. E. 1985. Normal-mode analysis of lateral diffusion on a bounded membrane surface. *Biophys. J.* 47:337–347.

Koppel, D. E. 1986. Fluorescence photobleaching recovery techniques for translational and slow rotational diffusion in solution and on cell surfaces. *Biochem. Soc. Trans.* 14:842–845.

Koppel, D. E., M. P. Sheetz, and M. Schindler. 1981. Matrix control of protein diffusion in biological membranes. *Proc. Natl. Acad. Sci. USA.* 78:3576–3580.

Lutz, H. 1978. Vesicles isolated from ATP-depleted erythrocytes of thrombocyte rich plasma. *J. Supramol. Struct.* 8:375–389.

Mohandas, N., and S. B. Shohet. 1978. Control of red cell deformability and shape. *Curr. Top. Hematol.* 1:71–125.

Pfafferot, C., R. Wenby, and H. J. Meiselman. 1982. Morphologic and internal viscosity aspects of rbc rheologic behavior. *Blood Cells (Berl.).* 8:65–78.

Reinhart, W. H., and S. Chien. 1986. Red cell rheology in stomatocyte-echinocyte transformations: roles of cell geometry and cell shape. *Blood.* 67:1110–1118.

Saffman, P. G., and M. Delbruck. 1975. Brownian motion in biological membranes. *Proc. Natl. Acad. Sci. USA* 72:3111–3113.

Schmid-Schonbein, H. 1981. Factors promoting and factors preventing the fluidity of blood. *In* Microcirculation, Current Physiologic, Medical and Surgical Concepts. R. H. Effros, H. Schmid-Schonbein, and J. Ditzel, editors, Academic Press Inc., New York. 249–269.

Schmid-Schonbein, H., and R. Wells. 1969. Fluid-drop like transition of erythrocytes under shear. *Science (Wash. DC).* 20:288–291.

Schmid-Schonbein, H., J. V. Gosen, L. Heinich, H. J. Klose, and E. Volger. 1973. A counter-rotating "rheoscope chamber" for the study of the microrheology of blood cell aggregation by microscopic observation and microphotometry. *Microvasc. Res.* 6:366–376.

Schmid-Schonbein, H., R. Grebe, and H. Heidtmann. 1983. A new membrane concept for viscous rbc deformation in shear: spectrin oligomer complexes as a Bingham-fluid in shear and a dense periodic colloidal suspension in bending. *Ann. NY Acad. Sci.* 416:225–254.

Sheetz, M. P. 1983. Membrane skeletal dynamics: role in modulation of red cell deformability, mobility of transmembrane proteins and shape. *Semin. Hematol.* 20:175–188.

Sheetz, M. P., and S. J. Singer. 1974. Biological membranes as bilayer couples. A molecular mechanism of drug-erythrocyte interactions. *Proc. Natl. Acad. Sci. USA.* 71:4457–4461.

Sheetz, M. P., M. Schindler, and D. E. Koppel. 1980. The lateral mobility of integral membrane proteins is increased in spherocytic erythrocytes. *Nature (Lond.).* 285:510–512.

Smith, D. K., and J. Palek. 1982. Modulation of lateral mobility of band 3 in the red cell membrane by oxidative cross-linking of spectrin. *Nature (Lond.).* 297:424–425.

Tank, D. W., E.-S. Wu, and W. W. Webb. 1982. Enhanced molecular diffusibility in muscle membrane blebs. *J. Cell Biol.* 92:207–212.

Tran-Son-Tay, R., S. P. Sutera, G. I. Zahalak, and P. R. Rao. 1987. Membrane stress and internal pressure in a red blood cell freely suspended in a shear flow. *Biophys. J.* 51:915–924.

Weir, M. L., and M. Edidin. 1986. Effects of cell density and extracellular matrix on the lateral diffusion of major histocompatibility antigens in cultured fibroblasts. *J. Cell Biol.* 103:215–222.

Weir, M. L., and M. Edidin. 1988. Constraint of the translational diffusion of a membrane glycoprotein by its external domains. *Science (Wash. DC).* 242:412–413.